2024 IEEE/ASME International Conference on Advanced Intelligent Mechatronics (AIM)
July 15-19, 2024. Boston, MA, USA

Model Identification of a Soft Robotic Eye Actuator for Safe Social Interactions

Algot Lindestam[1], Seshagopalan Thorapalli Muralidharan[1] *Student Member, IEEE*, Georgios Andrikopoulos[1] *Member, IEEE*, Randy Gomez[2] *Member, IEEE*

***Abstract*— This paper explores the model identification of a novel tendon-driven soft continuum actuator, intended as a functional joint for the social robot HARU. The actuator's design is customized for integration into HARU's eye joints, emphasizing safety in interactions with children, in accordance with UNICEF's "Policy Guidance on AI for Children". The performed experimental study assesses and compares the accuracy of various auto-regressive with exogenous inputs (ARX) modeling techniques—linear, nonlinear, and recursive—through motion data from dynamic experimental tests of the actuator under different orientations. The results provide insights into the efficiency of these modeling strategies in dynamic conditions with continuum actuators, thereby offering a basis for model selection in the integration of soft actuators into robotic systems for practical applications.**

I. Introduction

The field of social robots has witnessed a surge in growth and development over the last decade [1]. Given the potential upsides and ethical issues, the United Nations has issued a Policy Guideline document [2] outlining, the conditions necessary when developing and deploying robots and AI related products designed for children. In accordance with these policy guidelines, the robot platform HARU was developed [3], with the research goal of serving as a companion and educational robot for children.

As first presented in [3] and shown in Fig. 1 (left), HARU's design was characterized by a pair of eyes connected to the body through a neck structure. Over time, the robot has undergone modifications to improve the structure in terms of compliance, expressiveness and ability to interact safely with users and the surroundings [4]. One of the currently investigated modifications is the incorporation of soft actuators in the eyes and neck components to enable additional degrees-of-freedom (DOFs), as shown in Fig. 1 (right) and conceptually depicted in Fig. 2.

Structurally compliant actuators, a term used interchangeably with soft actuators, are devices that generate motion through structural deformation in the body of the actuator [5], [6]. While the structure and material provide compliance, motion in these actuators is often implemented using various methods, such as heat, air pressure (pneumatic), liquid pressure (hydraulic), mechanical (force), electrical (hydrogels), electrostatic, liquid crystals etc [7], [8]. These actuation methods vastly differ from each other with respect to actuation speed, power requirement, materials, manufacturability

[1]Robot Design Lab, Mechatronics Unit, KTH Royal Institute of Technology, SE-10044 Stockholm, Sweden
[2]Honda Research Institute of Japan Co. Ltd., 351-0188, Wako, Japan.
Corresponding Author's Email: geoand@kth.se

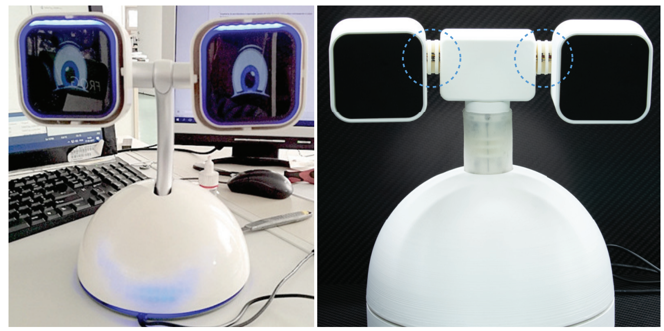

Fig. 1. (left) HARU as first presented in [3] and (right) the revised prototype structure incorporating soft joints in the head and eye structures, for enabling life-like motions and enhancing safety during interactions. This work is focused on the development and modeling of a soft continuum actuator for enabling the yaw motion of the eye structures (highlighted in blue and conceptually presented in Fig. 2).

etc. Most actuation methods of soft robots lack the forces required to actuate and move masses of significant weights and inertia (>200g). In addition to these, most methods also involve mass transport, which can typically be slower. Other methods require the use of external compressors or high voltage supplies, which tend to be bulky and energy intensive.

For HARU, wire-driven mechanical methods of actuation were selected, as they can provide fast and high actuation forces with relatively small components. In related literature, wire-driven actuators are known as Tendon-Driven Continuum Actuators (TDCA) and typically involve routing tendons along the robot's backbone, fixed at predefined locations, leading to the bending of the corresponding segment towards the tendon's direction when pulled.

The modeling of TDCAs usually involves distributed and lumped backbone parameterizations to describe the backbone's curvature and orientation [9]. However, the majority of related research has focused on static or quasi-static models, providing insights into steady-state conditions without significant external loads [10], [11]. These models typically assume that the actuator's shape can be described by a set of equilibrium equations neglecting dynamic effects such as inertia and damping, as for example piecewise constant curvature and state-space model representations [12], [13].

Recent efforts have also explored the use of autoregressive models with exogenous inputs (ARX) to capture the behavior of TDCAs [14], [15]. ARX models offered a promising modeling approach by incorporating past output values and

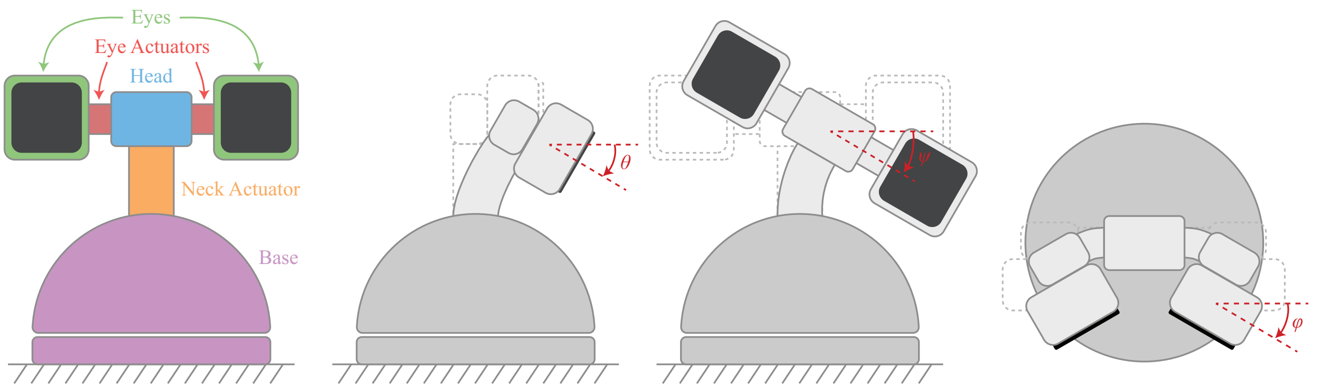

Fig. 2. Conceptual sketches of the re-imagined HARU platform. From left to right: HARU with highlighted main components, and its three dominant neck and eye degrees of freedom (neck pitch, neck roll, eye yaw).

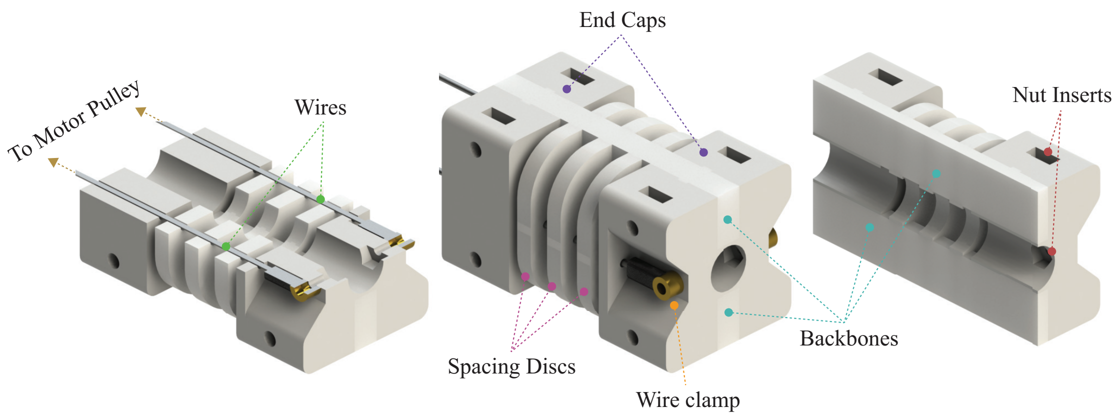

Fig. 3. Graphical representations of the soft continuum core with annotated design specifics: (middle) isometric view, (left-right) sagittal and transverse section views displaying the interior structure and tendon routing.

external inputs into the prediction of future states. However, these studies primarily validated the models under static conditions or with minimal external loading, limiting their applicability for dynamic scenarios influenced by loads and rapid movements in various inclinations [16], [17].

This limitation points to a gap in the literature, as dynamic conditions—where loads can change rapidly—are crucial for real-world applications of TDCAs. To this goal, the present paper performs a comparative study between linear, nonlinear, and recursive implementations of ARX models to provide valuable insights concerning a novel TDCA designed to operate in dynamic scenarios while under load. Through an experimental validation of the developed TDCA prototype, this work aims at contributing to a better understanding of the trade-offs between model complexity and accuracy.

The remainder of this paper is organized as follows: Section II provides an overview of the methods used to design the TDCA's core component and the model identification algorithms selected for the comparative study. Section III presents the main components of the TDCA prototype and provides information on the experimental setup used for the core's dynamic identification study. The comparative results and commentary related to the identification accuracy under the performed tests are given in Section IV. Finally, discussion points on the results are given in Section V and concluding remarks are provided in Section VI.

II. Methods

A. Continuum Core Design

The continuum core component's design underwent an iterative optimization process, aimed at achieving a balance between the application's requirements. These include satisfying spatial constraints for given robot body and eye compartments, reducing the overall weight to minimize inertia effects, enhancing the bending range, and ensuring that the torque required for these movements remains within the motor's capability. The design for the continuum core is conceptually presented in Fig. 3, focusing on the core mechanism of the TDCA composed of three spacing discs positioned between two mounting pieces. This assembly is supported by two backbone structures, ensuring structural integrity and bending functionality, while facilitating the passage of two wires through symmetrically aligned holes on the transverse plane of the discs and mounting pieces. These wires are securely clamped and anchored at one end of the core to prevent slippage during operation. The opposite ends of these wires are connected to a motor pulley whose rotational motion is converted into a force that induces a bending moment in the backbones. This mechanism allows for precise control over the actuator's range of bending angles and trajectories. To allow for attachment of the core to the robot's body and eye components, both end pieces are equipped with screw holes and respective cuts for nut inserts ensuring a secure and stable installation. Additionally, the core is designed with an internal cylindrical cavity for cable management, enabling routing of power and data wires from the eye components to the robot's main body.

B. Model Identification

Autoregressive models with exogenous inputs (ARX) are forms of polynomial models where the system output is a linear combination of previous inputs and outputs (called regressors). ARX models possess the ability to effectively capture the dynamic relationships between the actuator inputs and outputs while incorporating the influence of external factors or disturbances. This is particularly beneficial for TDCAs, which exhibit highly nonlinear and complex behaviors due to their flexible, continuously deformable structures. The ARX model, characterized by its simplicity and flexibility, allows for the inclusion of previous output values and current and past values of exogenous inputs, making it well-suited to model the dynamic interactions in TDCAs [18].

With $y(t)$ as the system output, $u(t)$ the system input and a_n and b_n constants determining the system order and behaviour, the output of the system is determined by a linear combination of the previous system states $y(t-n)$ and $u(t-n)$. These are called *regressors* (or lags) and are all contained in the *regression vector* φ. The parameters a and b are similarly be written as a parameter vector θ. A ARX model can, thus, be written as:

$$\begin{aligned}\varphi(t) &= [y(t-1), y(t-2), \ldots, y(t-n_a), \\ &\quad u(t), u(t-1), \ldots, u(t-n_b+1)] \\ \theta &= [-a_1, -a_2, \ldots, -a_{n_a}, b_1, b_2, \ldots, b_{n_b}]^T \\ y(t) &= \varphi(t)\theta\end{aligned} \tag{1}$$

When identifying this type, the "best fit" parameter vector is commonly found using the least squares method [19].

Building on linear ARX models, nonlinear ARX models (NARX) introduce nonlinear components and are particularly useful for capturing complex behaviors in systems where the current output depends on previous outputs and inputs [20]. The basis for these models is a modified equation 1 where a nonlinear mapping function F is used instead of a linear combination of the regressors:

$$\begin{aligned}y(t) = F\,(&y(t-1), y(t-2), \ldots, y(t-n_a), \\ &u(t), \ldots, u(t-n_b+1))\end{aligned} \tag{2}$$

Differing from a linear ARX model, the NARX model's regressors are not limited to linear combinations of the input-output variables, with polynomial or trigonometric functions of like $u(t-3)^2$ or $sin(y(t-1))^2$ being used. The regressors can, in theory, be set to arbitrary functions of previous inputs and outputs, but polynomials and trigonometric functions are among the more common nonlinear regressors [19], while for this work a wavelet network was used as F [21].

In the case of NARX, the parameter vector is calculated using numerical methods, which results in variable execution times making the models unsuitable for on-line identification. To amend this, the recursive form of the least squares algorithm is used to adapt the parameter vector to new data [19]. Such models are particularly useful for time-varying systems where the model parameters need to be adapted continuously to reflect changes in the process dynamics. In the recursive ARX (RARX) case, parameters $\{a_i\}$ and $\{b_i\}$ are updated at each time step based on new data, giving them a stronger influence on the parameter updates. The forgetting factor λ, where $0 < \lambda \leq 1$, modifies this process and it's applied to progressively reduce the weight of older data points in the error function that the parameter updates seek to minimize.

III. Experimental Setup

A. Continuum Core Development

The continuum core prototype, shown in Fig. 4 (top), was fabricated using Thermoplastic Polyurethane (TPU) with an 85A shore hardness on an FDM 3D printer (Raised 3D E2), with settings of 90% infill and 0.1 mm layer height. The design and material choice for the continuum core were iteratively optimized to minimize deflection angles, specifically the two passive degrees of freedom at the continuum joint's right end-cap (illustrated in Fig. 4 (top) and referred to as the TDCA's end-effector), under a target load of 0.4 kg placed 0.04 m from the end-effector.

Subsequently, two ends of a single plastic-coated multi-strand steel wire were secured and affixed to the core's end-effector. This wire was routed around a motor pulley fabricated from Polylactic Acid (PLA) using FDM 3D Printing. To achieve consistent and repeatable actuator performance, the use of an tightening rig facilitated the wire's routing and fixation, ensuring uniform tension across the system.

B. Setup Components

For the purposes of testing the TDCA and comparing the model performance, an experimental setup was designed and developed in different iterations. The setup iteration depicted in Fig. 4 (middle) enabled changing the load on the actuator's end-effector with removable weights, while the actuator's base remained at a zero pitch inclination. Microprocessing units were also used to control the motor's operation and read the actuator motion measured via an IMU.

For testing the TDCA under varying loads and base pitch inclinations (defined as neck pitch in Fig. 2), the setup was modified to support fixed (4 (bottom-left)) and manually adjustable (4 (bottom-right)) pitch variations. The fixed pitch was predetermined to ±22.5 and ±45 degrees, the latter value aligning with HARU's neck's maximum permissible pitch. In the manually adjustable pitch, the actuator assembly was affixed to two bearing carrier brackets.

In all setup iterations, the TDCA was loaded with 0.4 kg symmetrically placed at a longitudinal distance of 0.04 m

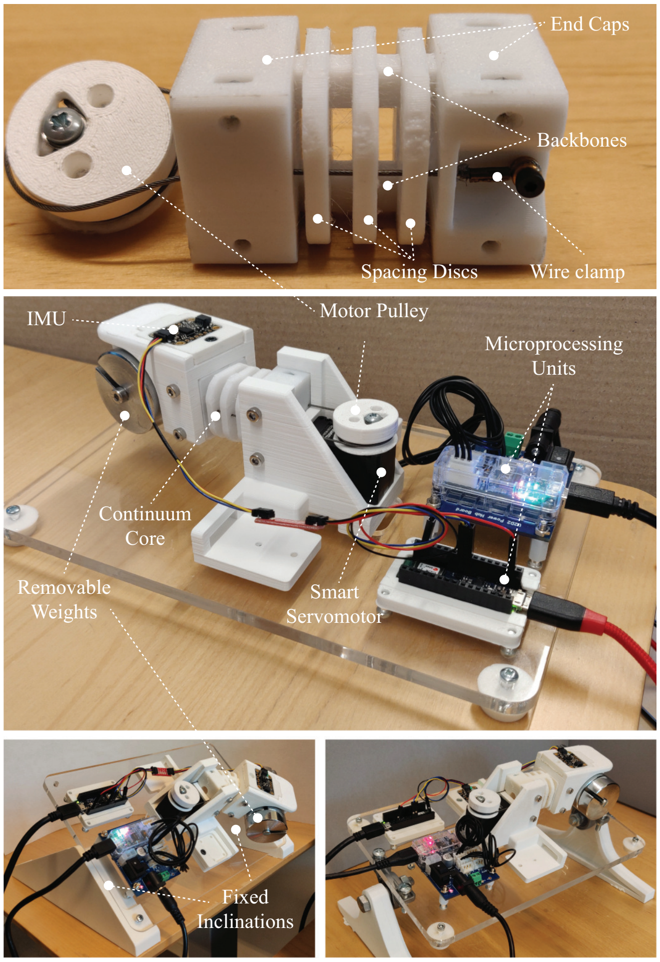

Fig. 4. (top) Continuum core prototype connected to the motor pulley via plastic-coated multi-strand steel wire. (middle) Setup used for testing and data acquisition of the actuator's performance. (bottom) Modified setup for enabling manually varied (bottom-left) and fixed (bottom-right) pitch variations for the actuator's model identification sequences.

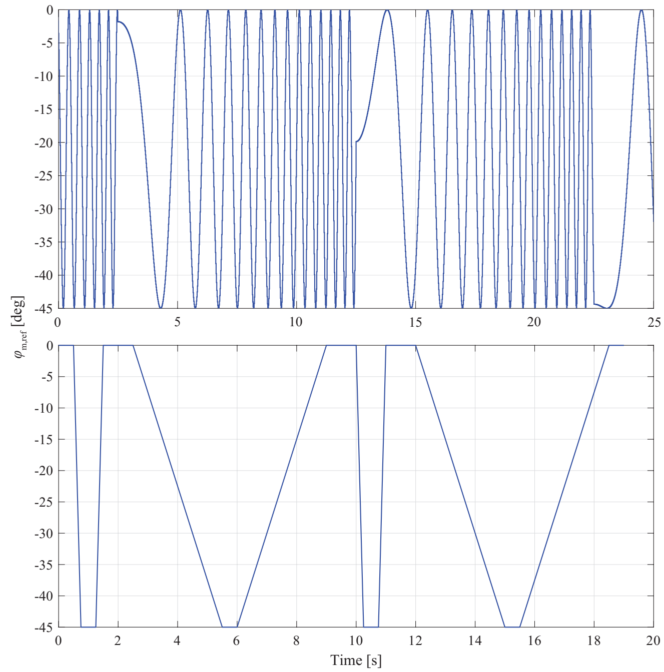

Fig. 5. Two period snippet of the signals used as input reference angles to the motor $\phi_{m,ref}$ for the identification of the continuum actuator: chirp (top), ramp-wise (bottom).

from the end-effector, both selected to match the current weight and center of mass of HARU's eye compartment (Fig. 1). A Dynamixel XC330 smart servomotor powered the TDCA, controlled and powered by a U2D2 microprocessing unit. A BNO055 IMU measured the end-effector's sensed orientation in Euler format, acquired via an Arduino Nano 33 IoT microprocessing unit. A second IMU was mounted on the actuator's base to serve as a reference frame (4 (bottom-right)). All components were mounted on an acrylic plate via connection parts designed and 3D-printed using PLA. All acquired data and control signals were managed through a personal computer running MATLAB and Simulink.

IV. Results

A. Validation Specifics

Initially, TDCA motion tests were conducted utilizing a unidirectional chirp signal for excitation, as illustrated in Fig. 5 (top), which was repetitively deployed to gather an extensive dataset. The signal's lower frequency was set at 0 Hz, while the upper frequency limit was established at two-thirds of the theoretical maximum (2.75 Hz), derived from the motor's no-load velocity.

Data pertaining to TDCA angular responses were collected at various discrete pitch angles (±45, ±22.5, 0 degrees) to document changes in system behavior attributable to orientation variations. The gathered data served as a foundation for the training of models to facilitate performance comparisons. These models were characterized by an identical number of lag terms in both input and output, with lags ranging from 0 to 4 being examined. The training of ARX and NARX models utilized data procured at a 0 degrees pitch, presumed to represent an optimal approximation for both positive and negative pitch angles. The RARX model underwent training on the identical dataset, yet it received individual training based on data from each pitch angle prior to testing. This approach enabled the model to adapt, potentially offering a superior fit compared to the non-adaptive ARX model.

The forgetting factor λ of the adaptive model was configured to 0.998, contingent upon the sampling interval t_s of 7 msec and a stipulated "memory" duration of 30 sec, aimed to encompass multiple cycles of the chirp signal and thereby facilitating expedited data acquisition. Data acquisition adhered to the protocol established for training data collection, which entailed the utilization of both the chirp signal and a ramp-wise signal. The latter incorporated movements at varying velocities, as illustrated in Fig. 5 (bottom).

To extend the validation of the trained models to dynamic motion scenarios, test sequences were conducted where the pitch of the setup was modified continuously. Such modifications more accurately reflect the operational context within the HARU robot, where actuator orientation undergoes dy-

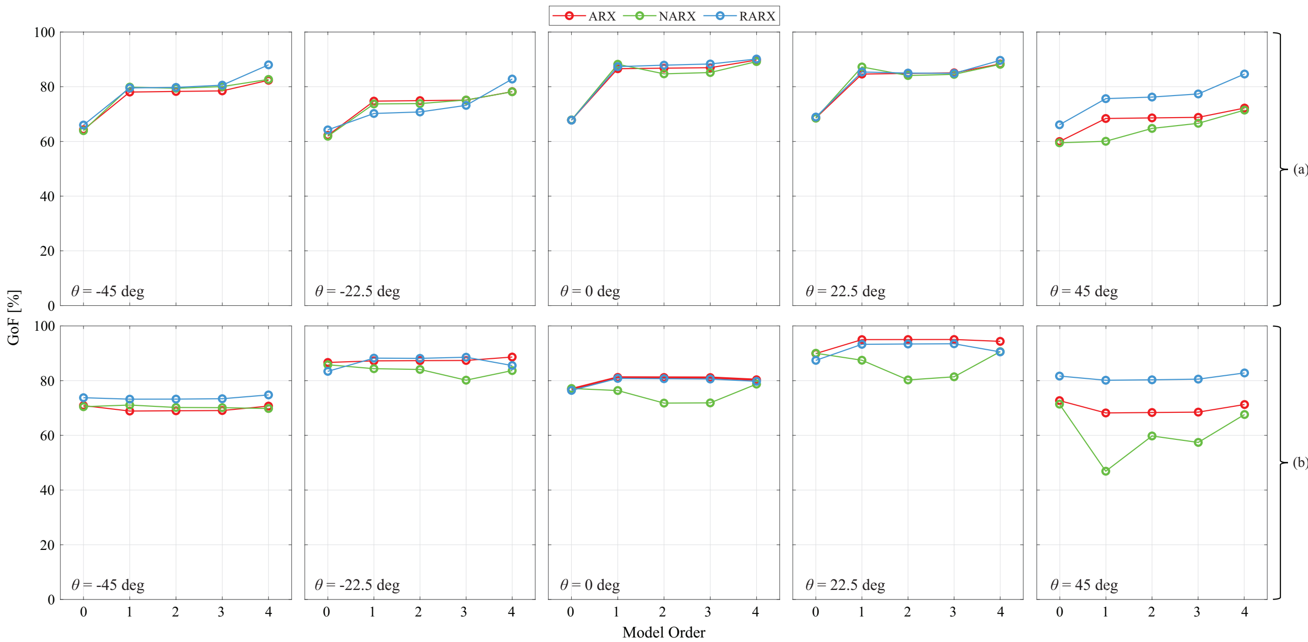

Fig. 6. Goodness of fit graphs for the three different models (ARX, NARX, RARX), model order (0–4) and discrete pitch angles (±45, ±25, 0 degrees) for the cases of the (a) chirp and (b) ramp-wise input reference angles.

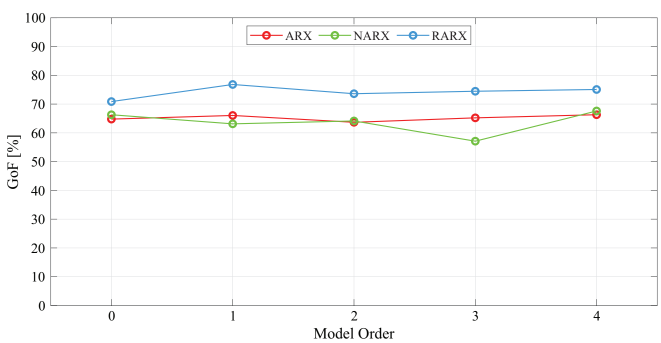

Fig. 7. Graph showing model fit for differing models and model order in the continuous pitch test.

namic adjustments concurrent with head movements. These tests were executed with the setup affixed to brackets of fixed inclination, as depicted in Fig. 4 (bottom-right). In this case, an additional IMU was installed at the base of the test rig to act as a reference frame for the end-effector's frame. Data collection occurred while manually adjusting the pitch angle across the full range of motion, with the chirp signal (Fig. 5) serving as a reference. The input and output data thus acquired were employed to compute simulated outputs for both the ARX and NARX models. For simulations involving the RARX model, the model underwent retraining with the newly acquired test data, with the parameter vector being logged at each time step. Utilizing this logged parameter vector and the system's initial conditions, a simulated output for the recursive RARX was also generated.

The efficacy of the evaluated models was determined through the application of the normalized root mean square error (NRMSE) between the simulated and the actual system outputs. This metric of error is delineated as the goodness of fit (GOF) in accordance with equation 3. The computation of GOF yielded the plots depicted in Fig. 6 and 7.

$$\%GoF = (1 - NRMSE) * 100 \tag{3}$$

B. Model Performances

The evaluation of ARX, NARX, and RARX models using the chirp signal for discrete pitch inclinations, as depicted in Fig. 6, demonstrates comparable performance across models. Notably, at a +45 degree pitch angle, RARX exceeds ARX and NARX by 7.5% in accuracy, with ARX marginally surpassing NARX. Ramp-wise validation signals, shown in Fig. 6 (b), reveal NARX's inferior performance relative to ARX and RARX models across pitch angles from -22.5 to 22.5 degrees. At 45 degrees, RARX's superiority is nearly 10%, close to the findings from the chirp signal evaluations, while NARX's accuracy declines to a 47% fit for a single lag term. Despite no explicit trend in the data, model accuracy diminishes at extreme angles, particularly where RARX significantly outperforms ARX and NARX at +45 degrees. This disparity is not observed at -45 degrees, where model performance is comparably aligned.

Further analysis involved model output comparison for varying pitch signals, with the aggregated comparative results for the three models shown in Fig. 7. GoF metrics appear generally lower than those from discrete angle assessments, with ARX and NARX yielding similar performances but inferior to RARX. Contrasting discrete pitch angle evaluations, model fits display consistency across increasing model orders. In summary, under dynamic conditions, RARX achieves the highest performance with a 70-80% fit, while ARX and NARX models lag with 60-70% fits.

V. Discussion

As depicted in Fig. 6, performance across examined models was consistent at pitch angles near 0 degrees, except NARX, which underperformed compared to ARX under certain conditions with signals of varied velocities (Fig. 6 (b)). Contrary to Parvaresh and Moosavian's findings [14], no advantage of NARX over ARX was observed for this TDCA design. The performance decline in nonlinear models, particularly with the ramp-wise signal, might suggest overfitting. However, this is unlikely as performance reduction does not escalate with model complexity, even when compared to chirp signals at the same angle.

The discrete angle tests revealed significant disparities in performance across +22.5 and +45 degree pitch angles. This variation can be attributed to dynamic changes between the pitch orientations tested, which rendered non-adaptive models ineffective. Consequently, these models exhibited diminished accuracy, a limitation not observed in RARX.

At positive pitch angles, the load's weight generates a moment that displaces the actuator from its center, potentially explaining the observed discrepancies in model performance. At +22.5 degrees, the weight's influence is minimal, allowing the actuator's bending moment to predominate and realign the system. However, at +45 degrees, the weight's influence intensifies, substantially altering actuator behavior and reducing the system's "self-centering" capability. This phenomenon suggests that both linear and nonlinear dynamics are impacted, disproportionately affecting the accuracy of NARX due to the integration of both dynamic aspects.

The continuous angle tests indicate RARX's superiority in capturing the dynamic behavior of the system, achieving the commendably high model fit of 70-80%. Compared to Parvaresh and Moosavian's outcomes [14], the fits in this study are generally lower, yet they closely align with Quevedo et al.'s results [15], who employed an adaptive ARX model for a fixed-orientation MIMO system.

VI. Conclusions

In this work, a comprehensive comparison study between linear, nonlinear, and recursive implementations of ARX models was performed, for modeling a novel Tendon Driven Continuum Actuator (TDCA) designed for dynamic operational scenarios as a functional eye joint of the social robot HARU. Through the experimental validation of the developed TDCA prototype under load and different setup inclinations, the objective of this study was to provide new insights on the trade-offs between model complexity and accuracy within such dynamic environments. For inclinations closely aligned with the ones used in the training sessions of the models, all model types exhibited comparable performance, achieving model fits between 80-90%. When considering actuator inclinations diverging from those used in training, the non-adaptive and nonlinear ARX models demonstrated diminished efficacy, with fits ranging from 60-70%, whereas the adaptive model sustained fits around 80%. In dynamic scenarios characterized by varying actuator orientations, adaptive ARX proved to be the most effective in modeling the actuator dynamics, with fits approximately at 75% (contingent upon the model order).

References

[1] B. Liu, D. Tetteroo, and P. Markopoulos, "A systematic review of experimental work on persuasive social robots," *International Journal of Social Robotics*, vol. 14, no. 6, pp. 1339–1378, 2022.

[2] K. P. Virginia Dignum, Melanie Penagos and S. Vosloo. (2021, Nov) "policy guidance on ai for children". [Online]. Available: https://www.unicef.org/globalinsight/reports/policy-guidance-ai-children

[3] R. Gomez, D. Szapiro, K. Galindo, and K. Nakamura, "Haru: Hardware design of an experimental tabletop robot assistant," in *Proceedings of the 2018 ACM/IEEE International Conference on Human-Robot Interaction*, ser. HRI '18. New York, NY, USA: Association for Computing Machinery, 2018, p. 233–240.

[4] G. Andrikopoulos, L. Hassler, and R. Gomez, "On the design of a soft robotic neck for the social robot haru," in *IEEE/ASME International Conference on Advanced Intelligent Mechatronics (AIM)*, 2024.

[5] D. Rus and M. T. Tolley, "Design, fabrication and control of soft robots," *Nature*, vol. 521, no. 7553, pp. 467–475, 2015.

[6] G. Andrikopoulos and G. Nikolakopoulos, "Humanoid robotic leg via pneumatic muscle actuators: implementation and control," *Meccanica*, vol. 53, no. 3, pp. 465–480, 2018.

[7] W. Li, D. Hu, and L. Yang, "Actuation mechanisms and applications for soft robots: A comprehensive review," *Applied Sciences*, vol. 13, no. 16, p. 9255, 2023.

[8] G. Andrikopoulos, A. Papadimitriou, A. Brusell, and G. Nikolakopoulos, "On model-based adhesion control of a vortex climbing robot," in *2019 IEEE/RSJ International Conference on Intelligent Robots and Systems (IROS)*, 2019, pp. 1460–1465.

[9] P. Rao, Q. Peyron, S. Lilge, and J. Burgner-Kahrs, "How to model tendon-driven continuum robots and benchmark modelling performance," *Frontiers in Robotics and AI*, vol. 7, 2021.

[10] R. J. Webster and B. A. Jones, "Design and kinematic modeling of constant curvature continuum robots: A review," *The International Journal of Robotics Research*, vol. 29, no. 13, pp. 1661–1683, 2010.

[11] D. Trivedi, C. D. Rahn, W. M. Kier, and I. D. Walker, "Soft robotics: Biological inspiration, state of the art, and future research," *Applied Bionics and Biomechanics*, vol. 5, no. 3, pp. 99–117, 2008.

[12] B. A. Jones and I. D. Walker, "Kinematics for multisection continuum robots," *IEEE Transactions on Robotics*, vol. 22, no. 1, pp. 43–55, 2006.

[13] S. T. Muralidharan, R. Zhu, Q. Ji, L. Feng, X. V. Wang, and L. Wang, "A soft quadruped robot enabled by continuum actuators," in *2021 IEEE 17th International Conference on Automation Science and Engineering (CASE)*. IEEE, 2021, pp. 834–840.

[14] A. Parvaresh and S. A. A. Moosavian, "Linear vs. nonlinear modeling of continuum robotic arms using data-driven method," in *2019 7th International Conference on Robotics and Mechatronics (ICRoM)*, 2019, pp. 457–462.

[15] F. Quevedo, J. Muñoz, J. A. Castano Pena, and C. A. Monje, "3d model identification of a soft robotic neck," *Mathematics*, vol. 9, no. 14, 2021.

[16] A. D. Marchese, K. Komorowski, C. D. Onal, and D. Rus, "Whole arm planning for a soft and highly compliant 2d robotic manipulator," in *2014 IEEE/RSJ International Conference on Intelligent Robots and Systems*. IEEE, 2014, pp. 554–560.

[17] F. Renda, M. Giorelli, M. Calisti, and M. Cianchetti, "Dynamic model of a multibending soft robot arm driven by cables," *IEEE Transactions on Robotics*, vol. 30, no. 5, pp. 1109–1122, 2014.

[18] B. W. Yuguo Chen, Tze Leung Lai, "Robust autoregression with exogenous input model for system identification and predicting," *Electronics*, vol. 10, no. 6, p. 755, 2021.

[19] L. Ljung, *System identification: Theory for the user*, 2nd ed. Philadelphia, PA: Prentice Hall, 1998.

[20] A. Parvaresh and S. A. A. Moosavian, "Linear vs. nonlinear modeling of continuum robotic arms using data-driven method," in *2019 7th International Conference on Robotics and Mechatronics (ICRoM)*, 2019, pp. 457–462.

[21] J. Sjöberg, Q. Zhang, L. Ljung, A. Benveniste, B. Delyon, P.-Y. Glorennec, H. Hjalmarsson, and A. Juditsky, "Nonlinear black-box modeling in system identification: a unified overview," *Automatica*, vol. 31, no. 12, pp. 1691–1724, 1995, trends in System Identification.